Effective connectivity under task and resting states: a DCM study

Kyesam Jung[1], Chongwon Pae[2], Karl Friston[3], Sungho Tak[4], Yoon-Kyoung Choi[5], Chan-A Park[4], Chaejoon Cheong[4,6], Hae-Jeong Park[1,3,5]

[1]Department of Nuclear Medicine, Yonsei University College of Medicine, Seoul, South Korea
[2]BK21 PLUS Project for Medical Science, Yonsei University College of Medicine, Seoul, South Korea
[3]The Wellcome Trust Centre for Neuroimaging, University College London, London, United Kingdom,
[4]Bioimaging Research Team, Korea Basic Science Institute, Cheongju-si, Chungcheongbuk-do, South Korea
[5]Department of Cognitive Science, Yonsei University, Seoul, South Korea,
[6]Department of Bioconvergence Analysis, Korea Basic Science Institute, Cheongju-si, Chungcheongbuk-do, South Korea

Corresponding Author:

Hae-Jeong Park, PhD

Professor, Department of Nuclear Medicine, Radiology, Psychiatry,

Yonsei University College of Medicine,

50 Yonsei-ro, Sinchon-dong, Seodaemun-gu, Seoul, Republic of Korea 120-752,

Tel.: 82-2-2228-2363; Fax: 82-2-393-3035

Email: parkhj@yonsei.ac.kr

Abstract

Although the relationship between resting-state *functional* connectivity and task-related activity has been addressed, the relationship between task and resting-state directed or *effective* connectivity – and its behavioral concomitants – remains elusive. We evaluated effective connectivity under an N-back working memory task in 24 participants using stochastic dynamic causal modelling of 7 Tesla fMRI data. We repeated the analysis using resting state data, from the same subjects, to model connectivity among the same brain regions engaged by the N-back task. This allowed us to: (i) examine the relationship between intrinsic (task-independent) effective connectivity during resting and task states, (ii) identify phenotypes of task-dependent effective connectivity across participants, and (iii) associate behavioral performance with the similarity between task-dependent effective connectivity and resting-state intrinsic connectivity within each phenotype. We found a strong correlation between intrinsic effective connectivity in the resting and task states over subjects but a marked difference between task related changes in effective connectivity and resting-state intrinsic connectivity. We further identified a strong clustering of individuals according to task-related changes in effective connectivity during the N-back task, which was not apparent in resting-state connectivity. In subjects with significant parieto-frontal connectivity, the similarity between effective connectivity during N-back task performance and resting-state connectivity was positively correlated with 3-back reaction times. This result implies that a greater change in context-sensitive coupling – from resting state connectivity – is associated with faster reaction times. In summary, task-dependent connectivity endows resting-state connectivity with a context sensitivity, which predicts task performance.

Introduction

The human brain at rest exhibits highly structured spontaneous or endogenous fluctuations in functional MRI signals (Biswal et al., 1995; Greicius et al., 2003; Lowe et al., 1998; McGuire et al., 1996; Raichle and Snyder, 2007). The temporal correlations between these fluctuations serves as a basis for estimating (resting-state) functional connectivity among distributed brain regions (Fox and Raichle, 2007) – an approach that has attracted an unprecedented interest from the imaging neuroscience community. One important question about resting-state connectivity is its relationship with connectivity induced by task performance. Previous studies have suggested a tight link between the resting-state connectivity (or distributed patterns of endogenous activity) with task-related brain activation or connectivity (Biswal et al., 1995; Cole et al., 2014; Cole et al., 2016; Krienen et al., 2014; Park et al., 2014; Smith et al., 2009; Tavor et al., 2016; Yeo et al., 2015). For example, Cole et al. (2016) showed that functional connectivity from resting-state fMRI (rsfMRI) could explain the interaction among brain areas during task performance. Tavor et al. (2016) also showed that task-evoked activation could be predicted by (task-free) features of rsfMRI and DTI data. According to these studies, resting-state connectivity may serve as a potential 'scaffold' that underwrites diverse configurations subserving the pertinent functions of a given task (Fox and Raichle, 2007). In doing so, task-induced neural activity may not engage resting-state networks directly but may contextualize them and selectively engage the components of resting-state or intrinsic networks. Accordingly, several studies have focused on the divergence of task-dependent functional connectivity from that of the resting-state (Corbetta et al., 2008; Elton and Gao, 2014; Hermundstad et al., 2013b).

However, it is not still clear whether resting-state connectivity is simply recapitulated or reconfigured to perform a task. Moreover, previous studies of the relationship between resting-state functional connectivity and task-related activity have been largely based on temporal synchrony between regional activities (quantified using Pearson correlation coefficients), which does not provide information about the directed causal coupling among brain regions (for review, see Park and Friston, 2013). Inferences about directed coupling call for effective connectivity analyses that identify network architectures in terms of causal relationships. Therefore, the relationship between effective connectivity during the task-state and effective connectivity in the resting-state is unresolved.

In the current study, we characterized the relationship between task and resting-state coupling in terms of effective connectivity. To estimate effective connectivity for both states, we used dynamic causal modelling (DCM), which assumes a bilinear model of neural dynamics and a hemodynamic response model of fMRI data (Friston et al., 2003). In particular, stochastic DCM (Friston et al., 2011; Li et al., 2011) can estimate effective connectivity from both task and resting-state time series (with and without experimental inputs) using the same model inversion scheme. Using stochastic DCM, we examined the relationship between task and resting-state connectivity, within the context of an N-back

task, for which many neuroimaging studies have identified the key brain regions involved (Barch et al., 2013; Honey et al., 2002; Manelis and Reder, 2014; Owen et al., 2005) – and for which a few DCM studies are available (Brodersen et al., 2014; Deserno et al., 2012; Dima et al., 2014; Schmidt et al., 2014). In this paper, we will use the phrase *intrinsic connectivity* to refer to the effective connectivity underlying intrinsic brain networks in rsfMRI – and the effective connectivity that is intrinsic to a task set during task fMRI, having modeled any changes in effective connectivity due to task-related processes (i.e., extrinsic or modulatory connectivity), such as working memory.

We further note that task performance may not be supported by a single configuration of connectivity. In other words, there may be a many-to-one (i.e. *degenerate*) mapping between connectivity and function (Edelman and Gally, 2001; Friston and Price, 2003; Price and Friston, 2002; Tononi et al., 1999). This means, to perform a given task, people may engage different connectivity architectures. Although direct evidence for this *network degeneracy* hypothesis has not been established, it may explain the inconsistent effective connectivity observed in group DCM studies of N-back task (Bernal-Casas et al., 2013; Deserno et al., 2012; Dima et al., 2014; Fonville et al., 2015). Furthermore, the plurality of plausible dynamic causal models in group studies of 2-back tasks (Dima et al., 2014) may reflect the possibility that multiple patterns of effective connectivity support the same task. Brodersen et al. (2014) identified three subgroups using DCM, which showed significant differences in positive and negative symptom severity in schizophrenia (as assessed by PANSS). This clustering was taken as evidence of subtypes; not only in terms of behavioral performance but also at the level of effective connectivity engaged by the task.

The purpose of this study was to investigate the relationship between task-related effective connectivity and resting-state effective connectivity, to examine phenotypes of task-related effective connectivity across participants and to associate behavioral performance with the divergence of task related changes in effective connectivity from resting-state intrinsic connectivity, within each phenotype. Crucially, we were concerned with establishing the construct validity of effective connectivity, in relation to behavior – and the predictive validity of resting-state intrinsic connectivity, in relation to task-related effective connectivity. We therefore conducted independent DCM analyses of the task- and resting-state fMRI data to: (i) test for similarities between the respective intrinsic connectivity estimates (using correlations over connections) and (ii) to quantify the divergence of task-related effective connectivity changes from the resting state intrinsic connectivity. This should be contrasted with a complementary approach, in which both task and resting state fMRI data were modeled within a single DCM. Although this would have allowed us to model the differences between task, baseline and resting connectivity, it would not have enabled us to demonstrate their similarity or predictive validity (i.e., the ability to predict intrinsic connectivity under a task set from independent resting-state effective connectivity estimates).

Methods

Participants

24 healthy right-handed participants (13 males; age = 22.9 ± 2.7 years) underwent N-back task and resting-state fMRI during contiguous sessions. All participants had no history of neurological illness and were right-handed according to the Annett's handedness questionnaire (Annett, 1970). This study was carried out under the guidelines established by the Institutional Review Board of Korea Basic Science Institute, and all participants provided written informed consent before participating.

N-back Task Design

Prior to their visit, participants practiced N-back tasks with a training video (lasting 8 minutes) that was created specifically for this experiment – and administered via email. The video consisted of examples for 0-back, 1-back, 2-back, and 3-back trials that were similar to the trials they had to perform during the experiment. After training, they completed an online questionnaire to report the subjective level of easiness and understanding of the task on a 5-point scale. Only participants that scored 4 or 5 on the questionnaire were recruited. Upon their visit for the fMRI experiment, participants were subject to an additional training session on a computer – to ensure that they thoroughly understood the N-back task.

The N-back task was presented in a block design, alternating between experimental and baseline conditions. The design conformed to a previous study (Dima et al., 2014). A series of digits, in black font, were displayed on a white background for 1.7 s each, which then disappeared for 0.3 s. The 0-back condition was used to control for task engagement and vigilance. In the 0-back condition, participants were instructed to respond by pressing a button whenever the target digit "3" was displayed. In the working memory conditions (1-, 2-, and 3-back), the target was defined as any digit that was identical to the digit presented 1, 2, or 3 trials back. There were 12 epochs in all, each lasting 30 s, and comprising 10 digits. The entire N-back experiment lasted for 360 s, with a total of 34 targets and 134 non-target stimuli. The reaction time (RT) was measured for correct hits. To avoid any systematic order effects, all conditions were pseudo-randomized.

Image Acquisition and Processing of N-back and Resting-state fMRI

Functional and structural MRI data were acquired using a 7-Telsa scanner (Intera Achieva; Philips Medical Systems, Best, The Netherlands). fMRI blood oxygenation level dependent (BOLD) signals were obtained using a T2*-weighted gradient echo-planar imaging (EPI) sequence (repetition time (TR) = 2000 ms; echo time (TE) = 17 ms; flip angle = 70 °; matrix = 128 × 128; voxel size = 1.5 × 1.5 × 3.6 mm^3; field-of-view (FOV) = 192 mm; 30 interleaved slices without slice gap). High-resolution structural images were acquired using a three-dimensional T1-weighted sequence (TR =

4.3 ms; TE = 1.93 ms; flip angle = 8 °; matrix = 320 × 320; voxel size = 0.75 × 0.75 × 0.75 mm^3; FOV = 240 mm; 320 slices).

Preprocessing of N-back task and resting-state fMRI was performed using SPM12 (http://www.fil.ion.ucl.ac.uk/spm/software/spm12/, Wellcome Trust Centre for Neuroimaging, London, UK). The first 5 scans of fMRI were discarded to ensure magnetic equilibration. The 183 EPIs for N-back and the 300 EPIs for resting-state (eye-closed) were preprocessed by correcting for acquisition delays over different slices. Correction for head motion involved realignment of all consecutive volumes to the first image of the session. The realigned images were then co-registered to T1-weighted images, which were used to spatially normalize the functional data into a template space using standard nonlinear transformations. Finally, all normalized images were smoothed using a 6 mm full-width half-maximum Gaussian kernel. Low-frequency drifts were removed using a high-pass filter with a cut-off frequency of 128 s. In the first (within-subject) level analysis, the six motion regressors from the realignment procedure were included to eliminate artefacts caused by head movement. Group-level activation was assessed using the usual random effect analysis at the second (between-subject) level. Activation at the group level – among four conditions (0-back, 1-back, 2-back and 3-back) – was tested using a factorial general linear model to generate statistical parametric maps (SPM).

To summarize time-series in task-related areas, we first determined group level effects from the local maximum in second-level SPMs of the conjunction of 2-back and 3-back versus 0-back effects (uncorrected $p < 0.01$). These maxima were located in the bilateral superior parietal lobule (SPL), bilateral superior frontal gyrus (SFG), bilateral middle frontal gyrus (MFG), left para-cingulate gyrus (PrCG), and the right insula (INS). Individual (subject-specific) 5 mm volumes of interest (VOI) were centered on the nearest local maximum – around the group level maxima – on the first-level conjunction SPM of 2-back and 3-back versus 0-back effects (uncorrected $p < 0.001$); each with an extent threshold of 100 continuous voxels. The principle eigenvariate of all voxels within each VOI was then used to summarize regional activity in both the task and resting-state time series for subsequent DCM.

Dynamic Causal Modeling

In order to estimate effective connectivity, we used DCM for fMRI (Friston et al., 2003), which formulates neuronal dynamics in terms of bilinear approximations and hemodynamic responses using an extended balloon model (Buxton et al., 1998; Friston et al., 2003). The neuronal model for a deterministic DCM can be expressed as the following ordinary differential equation:

$$\dot{x} = \left(A + \sum_{j=1}^{J} B_j u(j) \right) x + Cu \qquad (1)$$

Here, x represents the hidden neural state for each region with dimension $n \times 1$ and u represents a $j \times 1$ vector of experimental inputs. The weighted undirected *adjacency matrix* A is $n \times n$ matrix for an *intrinsic connectivity* and B_j is the j-th $n \times n$ *condition-specific connectivity* matrix that is added to the intrinsic connectivity in an input or task-dependent fashion. C denotes an $n \times j$ matrix encoding the influence of experimental input on the hidden neural states. The neural state then passes through a hemodynamic response function $h(x, u, \theta_h)$ with hemodynamic parameters θ_h (Stephan et al., 2007). Finally, the BOLD signal, y, can be modeled as a mixture of the predicted response and observation error:

$$y = h(x, u, \theta_h) + e \tag{2}$$

Here, e is a normally distributed error term. Stochastic DCM differs from deterministic DCM (Eq. 1) in that it includes endogenous or random fluctuation ω (Chang and Lin, 2011; Daunizeau et al., 2012). Under a stochastic DCM, Eq. (1) can be rewritten as

$$\dot{x} = \left(A + \sum_{j=1}^{J} B_j u(j) \right) x + Cu + \omega \tag{3}$$

The driving input matrix C was specified to assign each item presented – in all conditions – as an input to the bilateral SPLs. A condition specific B matrix was assigned to all connections and modeled the effects of N-back items presented during either 2- and 3-back conditions. In this setting, the A matrix of the N-back task is not resting-state effective connectivity but effective connectivity intrinsic to the whole task, in the absence of modulatory 2-back or 3-back working memory effects. We used a fully connected model for an intrinsic connectivity matrix A and modulatory connectivity matrix B. We first inverted a deterministic DCM, to evaluate the initial parameters of the stochastic DCM (using the same connectivity model).

For a resting-state, the neuronal dynamics in Eq. (3) can be simplified, to a stochastic differential equation with an intrinsic connectivity matrix A, and a hidden state x, driven by endogenous stochastic fluctuations ω.

$$\dot{x} = Ax + \omega \tag{4}$$

In this setting, the adjacency matrix A mediates intrinsic brain networks. To initialize the parameters for stochastic DCM of the rsfMRI data, we used a spectral DCM as the deterministic homologue (Friston et al., 2014). Spectral DCM estimates effective connectivity among brain regions by

estimating effective connectivity and the spectral density of endogenous fluctuations using the observed complex cross spectral density over regions. We now turn to inferences about differences in effective connectivity within and between subjects.

Parametric Empirical Bayesian (PEB)

We conducted group (between-subject) level inference for DCM using the parametric empirical Bayesian scheme in SPM12. This allows one to specify between-subject linear models at the second level. A detailed explanation can be found in (Friston et al., 2015; Friston et al., 2016). Briefly, the first (within-subject) estimates are summarized in terms of posterior expectations and covariances and are passed to a second (between-subject) level to estimate posterior expectations and covariances of group means and other between-subject effects. At the second level, we used a general linear model with between-subject effects β on within-subject effects $\theta = \{A, B, C, \theta_h\}$ encoded by a design matrix X.

$$\begin{aligned} y_i &= \Gamma(\theta_i) + \varepsilon_i^{(1)} \\ \theta &= (I \otimes X)\beta + \varepsilon^{(2)} \end{aligned} \tag{5}$$

Here, Γ is a function that returns the predicted observations as a function of the model parameters (corresponding to Eq. (2) and (3) for task fMRI and Eq. (2) and (5) for rsfMRI). This hierarchical or parametric empirical Bayes model means that the parameters θ_i of the ith subject are modeled as a group average, plus a random effect $\varepsilon^{(2)}$. In the current study, we used a simple between-subject design matrix $X = [1 \dots 1]^T$, rendering β group means. Note that this PEB model furnishes estimates of group means and subject-specific (connectivity) parameters θ_i that are optimally shrunk to the group mean.

Post hoc analyses of connectivity

To define *similarity* between the effective connectivity induced under the N-back task and resting-state in each individual, we used the Pearson's correlation coefficient for three pairs of connectivity matrices; 1) the correlation between intrinsic connectivity A under N-back task and resting-state 2) the correlation between changes in connectivity B under the N-back task and intrinsic resting-state connectivity A and 3) correlation between the task related connectivity A + B under the N-back task and intrinsic resting-state connectivity A. The correlations were calculated for each subject– both including and excluding self or recurrent connections (effective connections on the leading diagonal of connectivity matrices).

Because the A matrix encodes the intrinsic connectivity and the B matrix encodes the changes in connectivity (induced by condition or working memory effects), the sum of the A and B matrix can

be associated with the effective connectivity expressed during the (working memory) conditions. Furthermore, note that the intrinsic (within-region) connections, along the leading diagonal of the A matrix, are log scale parameters in DCM for fMRI. This contrasts with the extrinsic (between-region) connections on the off-diagonal elements, which parameterize effective connectivity directly in terms of Hz. In other words, the within and between node connections have slightly different parameterizations (i.e., the log of a negative self-connection versus the connectivity between different regions). However, both have a prior expectation of zero and, in the absence of any structured connectivity, should show no correlation when estimated from independent data.

To characterize systematic between-subject variability in responses to the working memory tasks, we clustered individuals according to cross-subject similarity (correlation coefficient) matrix of the N-back connectivity matrix B, using a modularity optimization function in the brain connectivity toolbox (Leicht and Newman, 2008; Rubinov and Sporns, 2010), from which the maximum modularity (indexed as Q) was obtained (Newman and Girvan, 2004). For each subgroup or cluster, we performed *post hoc* PEB of the N back DCM. For completeness, this *post hoc* subgroup analysis was also applied to the resting-state connectivity.

Finally, to test for associations between effective connectivity and behavioral performance across subjects, similarities between the B matrix of N-back and the A matrix of resting-state were correlated with the RTs of subjects with nontrivial 3-back task performance (over 0.70 in recall rate). Figure 1 summarizes the procedure for the current analysis.

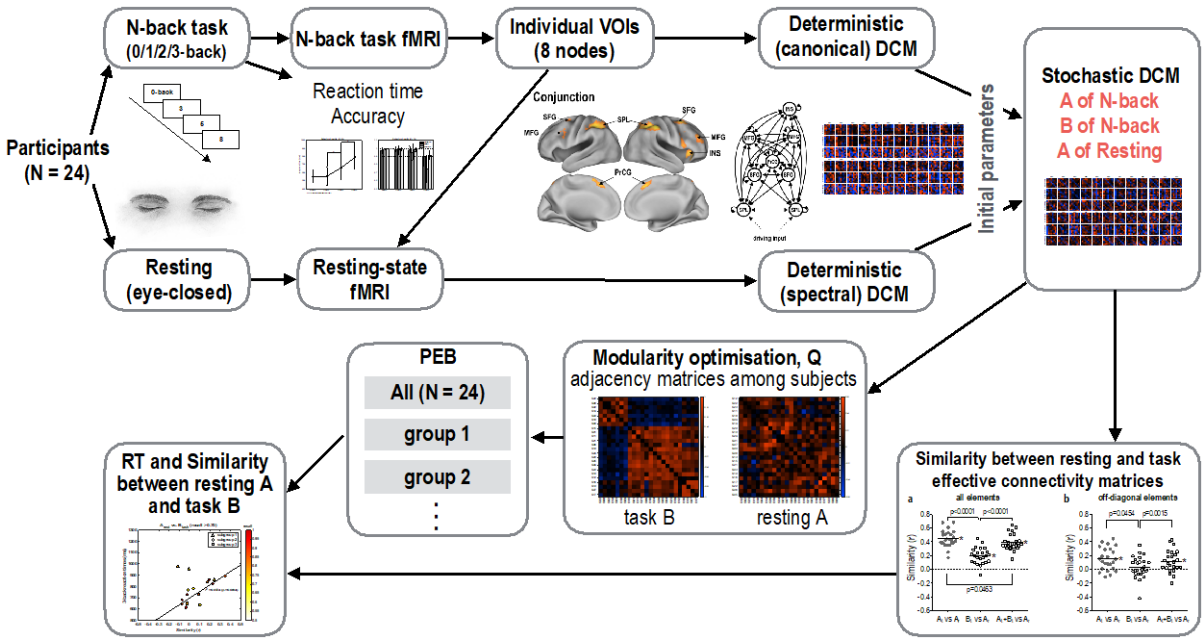

Figure 1. Procedure for DCM of resting-state and N-back task fMRI.

Results

Different Performance by N-back Task Difficulty

Mean and standard deviation of the RTs during 0-, 1-, 2-, and 3-back trials were 556.48 (74.27), 557.79 (113.98), 662.21 (146.39), and 792.24 (149.95) ms, respectively. The differences between group mean RTs were significant (p of 0-back vs. 2-back = 0.0012, p of 0-back vs. 3-back < 0.0001, p of 1-back vs. 2-back = 0.0007, p of 1-back vs. 3-back < 0.0001, p of 2-back vs. 3-back = 0.0059) except for the mean RT of 0-back vs. mean RT of 1-back. The accuracy, recall, and precision four all conditions were over 90%, except recall of 3-back condition (Table 1).

Table 1. Reaction time, accuracy, recall, and precision for each condition. Significance was assessed by paired t-tests (significance level = 0.05).

conditions	reaction time (ms)	accuracy	recall	precision
0-back	556.48 (74.27)	0.996 (0.007)	0.995 (0.018)	0.979 (0.036)
1-back	557.79 (113.98)	0.992 (0.023)	0.980 (0.059)	0.990 (0.034)
2-back	662.21 (146.39)†	0.987 (0.027)	0.954 (0.105)	0.986 (0.049)
3-back	792.24 (149.95)†‡	0.921 (0.059)	0.752 (0.171)	0.906 (0.131)

†: Significantly longer than 0-back and 1-back, ‡: Significantly longer than 2-back

Regions-of-Interest for N-back Task

In order to find common coordinates for both 2-back and 3-back, we conducted a conjunction analysis (Friston et al., 2005; Price and Friston, 1997). Figure 2a, 2b, and 2c show brain regions activated during the N-back task (conjunction analysis of 2-back and 3-back versus 0-back), which were subsequently used as nodes in the DCM analysis. The regions engaged by the task were the left superior parietal lobule (SPL; -42, -50, 56), right SPL (38, -52, 50), left superior frontal gyrus (SFG; -28, 2, 60), right SFG (28, 2, 58), left middle frontal gyrus (MFG; -44, 28, 30), right MFG (42, 38, 32), para-cingulate gyrus (PrCG; 0, 16, 50), and the right insula (INS; 34, 20, 0). Based on these coordinates, we summarized regional activity in both task-state and resting-state fMRI time series using (subject-specific) principal eigenvariates.

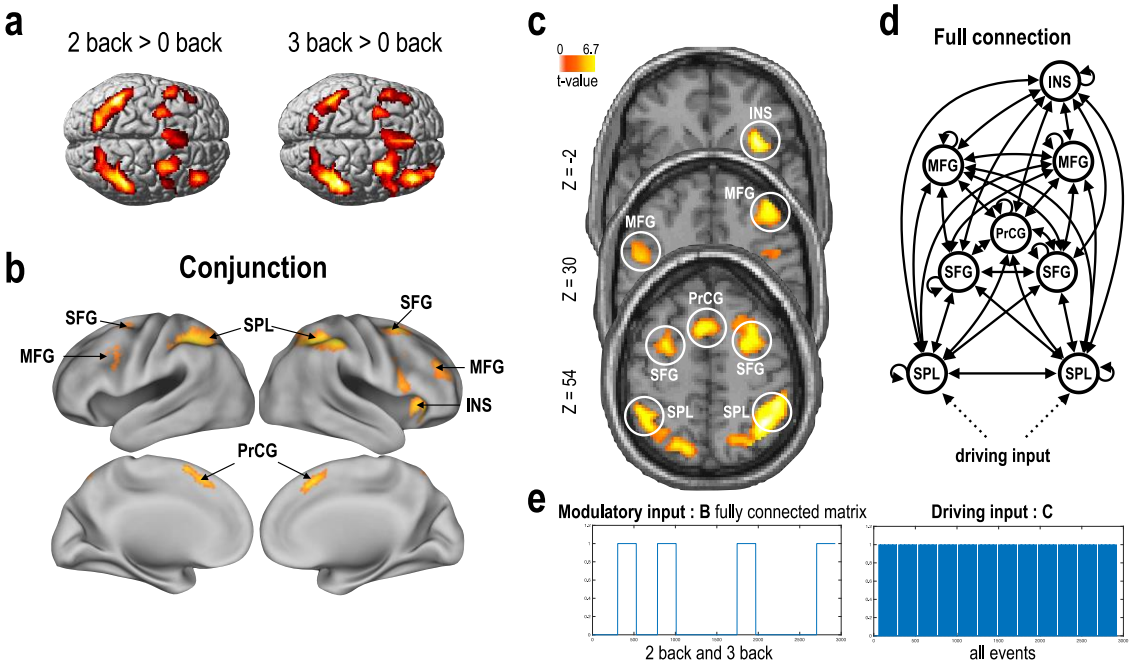

Figure 2. DCM model construction. (a) Group-level (positive) SPM of 2-back and 3-back effects against 0-back. (N = 24, uncorrected p<0.001, cluster size over 100 voxels). (b and c) Group-level SPM evaluated by a conjunction analysis of 2-back and 3-back versus 0-back effects (N = 24, uncorrected p<0.01, clusters over 100 voxels). Individual activations, corresponding to the group-level activations, were visually identified in the conjunction SPM of 2-back and 3-back versus 0-back effects. From individual VOIs, both task-based and resting-state fMRI time series were extracted. (d) The graph shows the fully connected DCM with 8 VOI or nodes. (e) Driving inputs from stimuli in all conditions were assigned to the bilateral SPL and task-dependent (working memory) effects of 2-back and 3-back conditions were assigned to every connection. SPL: superior parietal lobule, SFG: superior frontal gyrus, MFG: middle frontal gyrus, PrCG: para-cingulate gyrus, and INS: insula.

Stochastic DCM

Figure 3 shows the estimated stochastic DCMs for the N-back and resting-state of all participants. In the present study, three effective connectivity matrices were estimated, A (intrinsic) of N-back, B (working memory) of N-back, and A (intrinsic) of resting-state.

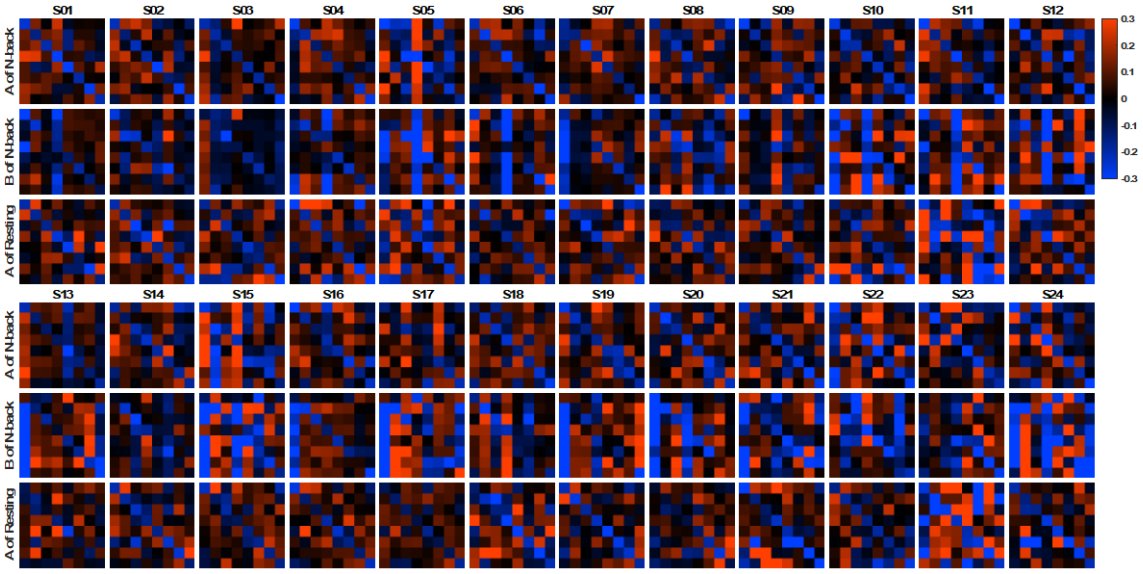

Figure 3. Subject specific effective connectivity matrices following stochastic DCM of the N-back and resting-state fMRI. 'A' and 'B' matrices correspond to intrinsic and condition related changes in effective connectivity. Each matrix element represents effective connectivity among 8 nodes in the following order: left SPL, left SFG, left MFG, right SPL, right SFG, right MFG, PrCG, and right INS. Directions are represented from columns to rows, meaning that the direction of an element (n, m) of the connection matrix is effective connectivity from the *m*-th region to the *n*-th region.

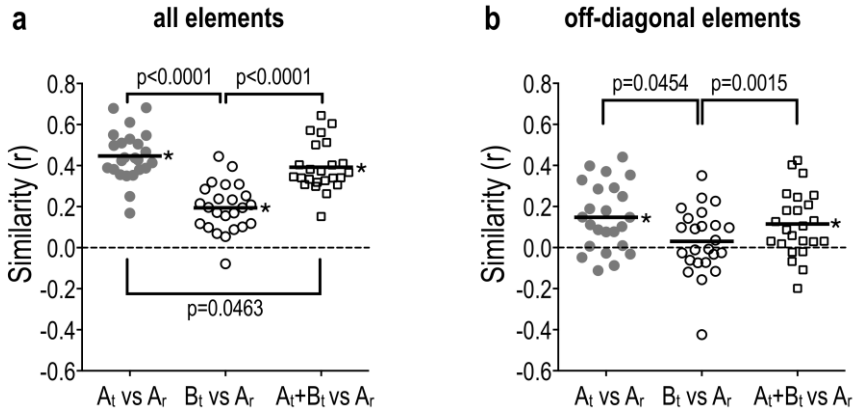

Figure 4. Similarity between N-back and resting-state. (a) correlations between all elements of the connection matrices are displayed. 'A_t vs. A_r' represents the correlation between effective connections from the N-back and resting-state. 'B_t vs. A_r' shows similarity between connectivity changes during N-back and the intrinsic connectivity during the resting-state. 'A_t+B_t vs. A_r' represents correlations between the effective connectivity during working memory conditions and the connectivity of the resting-state. (b) this panel uses the same format that tests for correlations among off diagonal elements of the connectivity matrices. Significant differences in correlations over subjects were tested using paired t-tests. Except for off-diagonal correlations between B_t and A_r, all correlations were significantly positive (using a one sample t-test against a null hypothesis of zero correlation). * indicates a significantly positive correlation ($p < 0.05$).

Similarity of effective connectivity between task and resting states.

The correlations between the resting-state connectivity A matrix and task-state A, B, and A+B were (nearly) all positive in every subject (and significantly positive when averaged across sub-

jects using one sample t-test: Figure 4a). These positive correlations were preserved when omitting self-connections: positive correlations between resting-state and N-back off-diagonal connections were significant across all subjects except for the case of B of N-back versus A of resting-state (Figure 4b). Correlations between the A connections of N-back and resting-state were significantly stronger than the correlations between changes in B connections during N-back and A connections during the resting-state. The correlations between connectivity during working memory A+B in the N-back and A connections of the resting-state were also significantly higher. These differences were also evident in the analysis with only off-diagonal elements (Figure 4b).

Differences among N-back Task and Resting-state connections

PEB estimates of effective connectivity in the N-back task showed that the group connectivity differed from zero for every connection (at 95% posterior confidence). A subsequent cluster analysis of subject-specific connectivity reveals three different clusters or subgroups. Figure 5a shows an optimized community structure based on the B connectivity matrix during the N-back task. The modularity Q of the optimized community structure was 0.3922. PEB estimates of connectivity within each subgroup revealed different intrinsic connectivity patterns (Figure 5b). The connectivity in subgroup 1 did not reach the confidence level (95%). In subgroup 2, however, 4 edges from the right SPL to bilateral SFG, PrCG, and left MFG were significant. Subgroup 3 had also 6 significant connections, which were from the left SPL to bilateral SFG, bilateral MFG, PrCG, and right SPL (see graphical illustrations of Figure 5c). For subgroups 1, 2, and 3, the mean and standard deviations of recall performance were 0.6961 (0.1769), 0.7991 (0.1717) and 0.6944 (0.1457), respectively. There was no significant group difference in recall. RTs of the three subgroups were 869.35 (200.81), 752.76 (116.02) and 785.60 (157.11) ms. The RT of subgroup 2 tended to be shorter than that of subgroup 1 ($p = 0.057$). When we consider subjects with good recall performance (recall > 0.7), RT was significantly shorter in subgroup 2 than in subgroup 1 ($p = 0.034$).

The community structure for resting-state DCMs, based on the between-subject similarity of the off-diagonal elements of the resting-state A matrix is shown in Figure 6. We found two clusters or subgroups but with very low modularity ($Q = 0.1871$). Their corresponding PEB results are shown in Figure 6b. There was no significant difference in mean RT between the two subgroups based on resting-state effective connectivity estimators.

Group differences between pattern similarities of A connectivity in the N-back task relative to of resting-state connectivity (A_t vs. A_r), and changes in connectivity during N-back relative to intrinsic resting-state connectivity (B_t vs. A_r) are shown for all subgroups in Figure 7a-7c. In the case of N-back, although the similarity of all elements showed a significant difference between 'A_t vs. A_r' and 'B_t vs. A_r', the similarity of the off-diagonal elements did not show any significant difference ($p < 0.05$).

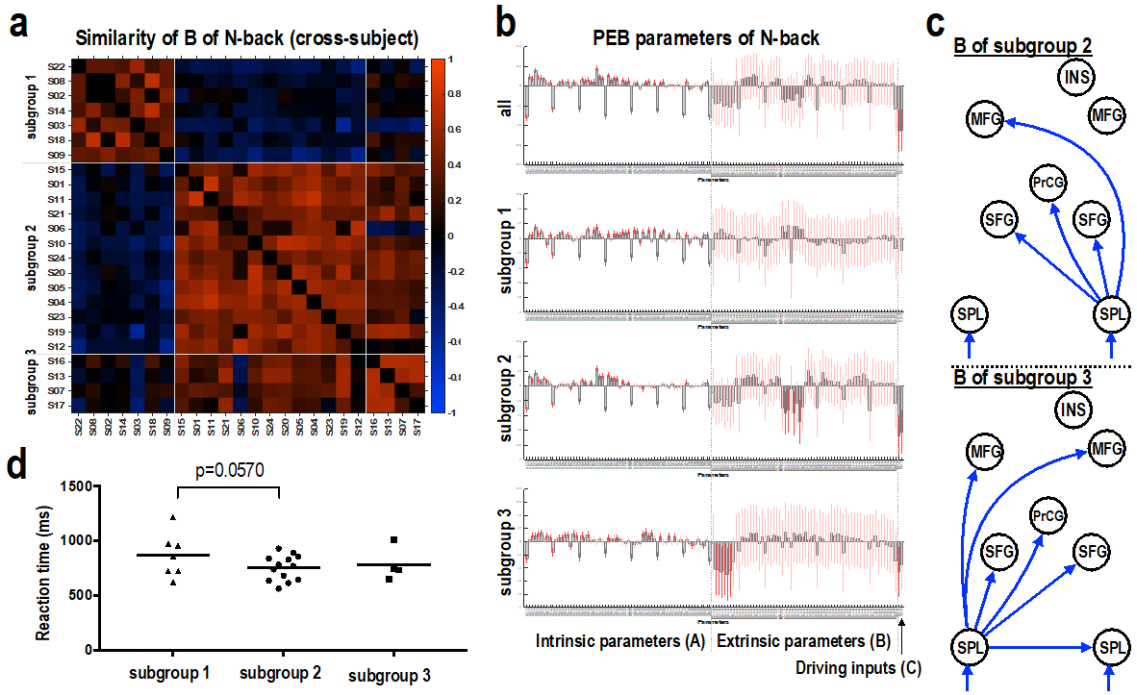

Figure 5. Three different subgroup were identified by modularity optimization of the adjacency matrix based on the between-subject similarity of the B matrices of N-back (Q = 0.3922) (a). Off-diagonal elements of the B matrix of each individual were used for computing pattern similarity. (b) subgroup level effect sizes of N-back DCMs for all the subjects and for the PEB estimates of the three subgroups. (c) Significant connectivity B and C (to the bilateral SPL) during the N-back task for subgroup 2 and subgroup 3 are displayed (confidence interval $p < 0.05$). There was no significant effective connectivity in subgroup 1. Blue arrows indicate negative effective connectivity. (d) The reaction times of 3-back task in subgroup 2 tended to be shorter than those in subgroup 1.

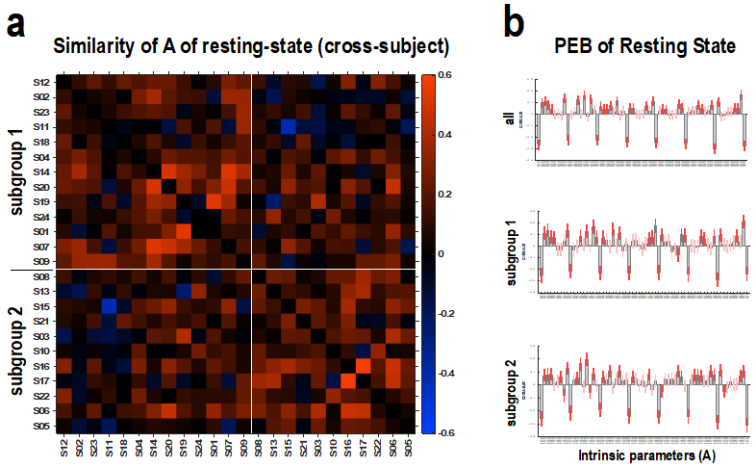

Figure 6. Modularity optimization of the adjacency matrix based on the between-subject similarity of the resting-state A matrix (off-diagonal part). The very low modularity index indicates weakly separable clusters (Q = 0.1871). Effective connectivity in the resting-state DCMs for each group was estimated by PEB.

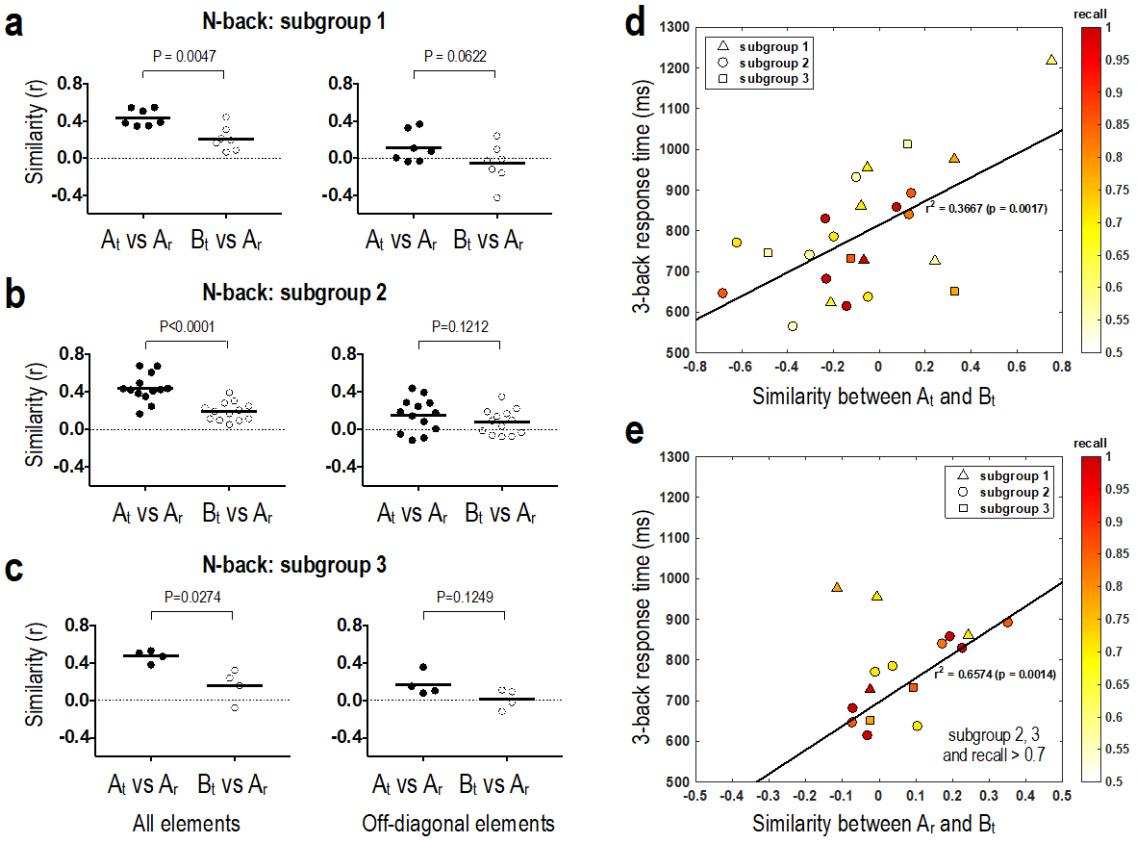

Figure 7. Similarity of the effective connectivity matrices for three subgroups clustered according to the associated B matrix (a-c) and their relationships with the reaction time (d and e). A_t vs. A_r shows the correlation between A connections from N-back task and resting-state. B_t vs. A_r shows the correlations between an N-back matrix B_t and a resting state matrix A_r. P indicates p-values after paired t-test. (d) 3-back reaction times were highly correlated with the similarity between A_t and B_t of the N-back task ($r = 0.61$, $p = 0.0017$). Triangles, circles and rectangles indicate three groups, while colors indicate recall rate. (e) The similarity between B_t of the N-back task and A_r of the resting state showed a significant correlation with 3-back reaction times in the subjects belonging to subgroups 2 and 3, who showed good task performance (chosen with a criterion of recall rate in 3-back > 0.7, $N = 12$, $r = 0.81$, $p = 0.0014$).

Association between Pattern Similarity and Behavior

As shown in Figure 7d, the similarity between resting state A and N-back B connectivity matrices were highly correlated with reaction times ($r = 0.61$, $p = 0.0017$). Figure 7e shows that this correlation remained significant for subjects in subgroups 2 and 3 and who showed good performance (recall rate over 0.7 in 3-back, $r = 0.81$, $p = 0.0014$).

Discussion

The main purpose of this study was to explore the relationship between effective connectivity during resting-state and task performance. In contrast to most previous studies that have associated functional connectivity during the resting-state with task-related activity patterns (Biswal et al., 1995; Cole et al., 2014; Cole et al., 2016; Krienen et al., 2014; Smith et al., 2009; Tavor et al., 2016; Yeo et

al., 2015), we explored both resting and task 'connectivity' among the same brain regions. Furthermore, instead of examining correlation-based functional connectivity, we used effective connectivity for both resting and task states. By utilizing stochastic DCM of resting-state and N-back task fMRI data, from the same brain regions, we showed a strong correlation between intrinsic effective connectivity in the resting and task states over subjects but a marked divergence of task-related changes in effective connectivity from resting-state intrinsic connectivity. Crucially, when task-related increases in connectivity correlated with the intrinsic connectivity in the N-back task – or the intrinsic connectivity during resting-state – reaction times increased. In other words, participants whose working memory related changes in connectivity diverged from baseline or resting-state connectivity patterns performed better on working memory tasks. Finally, we found a strong clustering of individuals according to effective connectivity during the N-back task, which was not found in the resting-state connectivity. This clustering – into phenotypic subgroups – had predictive validity in relation to performance.

Brain activity and connectivity during the N-back tasks

In the current study, we constructed DCM networks of brain regions engaged by the N-back tasks to relate resting-state and task-state effective connectivity. In general, the N-back task is known to recruit the parieto-frontal circuitries (Deserno et al., 2012; Dima et al., 2014; Owen et al., 2005; Park et al., 2011; Schmidt et al., 2014) including the bilateral SFG, bilateral MFG as well as other brain regions; such as right INS, and left PrCG (Barch et al., 2013; Manelis and Reder, 2014). Activations detected during the N-back tasks in the current study were consistent with the findings of these previous studies (Figure 2).

The current results are also consistent with Dima et al. (2014), who reported effective connectivity from the parietal regions to the frontal regions that differed across conditions (1-, 2-, and 3-back tasks). This previous study pre-specified several hypothesized models with a single effective connectivity of the parieto-frontal lobe and conducted a model comparison of the hypothesized models. The present study differs from Dima et al. (2014) in that we found effective connectivity from the parietal lobe to the frontal lobe, based on a full connection model.

Divergence of task-related effective connectivity from the resting-state intrinsic connectivity

As shown in Figure 4, the connectivity B during the task-state (2-back and 3-back) diverges greatly from the resting-state connectivity, whereas the intrinsic A connectivity manifests a similar pattern to that of intrinsic resting-state connectivity. Since the 0-back task used in this study is not an absolute resting-state but a baseline (incidental) task, the intrinsic connectivity matrix of the N-back task is not the same as the intrinsic connectivity of the rsfMRI. However, according to previous studies, most regions involved in the 0-back task do not overlap with the regions for 2- or 3-back conditions. Although an increased activation for the 0-back task compared to resting-state were found in the

right MFG (Papma et al., 2012), no activations were found in the left MFG during the 0-back condition (Harvey et al., 2005). The similarity between A of N-back condition and A of resting-state might be interpreted in this respect. Therefore, we can consider the A matrix of N-back as an intrinsic connectivity during the task, that is very similar to resting-state intrinsic connectivity. The similarity between A of N-back and A of resting-state serves as a reference for interpreting changes in connectivity during the N-back task in relation to intrinsic, resting-state connectivity.

We found a smaller similarity (i.e. correlation) between task-related connectivity changes and intrinsic resting-state connectivity, which reflects task-dependent and context-sensitive modulations of effective connectivity. Although a strong relationship between the intrinsic connectivity (or distributed spontaneous activity patterns) and task-related connectivity (or task-evoked activity patterns) has been reported (Biswal et al., 1995; Cole et al., 2014; Cole et al., 2016; Krienen et al., 2014; Park et al., 2014; Smith et al., 2009; Tavor et al., 2016; Yeo et al., 2015), intrinsic connectivity during the resting-state does not appear to be recapitulated but modulated or 'repurposed' to perform a specific task.

This interpretation of the current results is consistent with previous studies suggesting divergence of task-related connectivity from that of the resting-state. Corbetta et al. (2008) reviewed that the brain can *reorient* an attentive state via a deactivation of brain regions for default network from resting-state. Elton and Gao (2014) showed divergence between a network of selective attention task and that of resting-state. Moreover, functional connectivity changes during attention and memory tasks appear to facilitate diverse cognitive functions and disclose their context-sensitivity (Hermundstad et al., 2013a). The current study further shows that task-related connectivity during the N-back task diverges from the resting-state intrinsic connectivity and that the divergence was positively correlated with behavioral performance.

Group heterogeneity in N-back task effective connectivity

Behavioral performance in working memory tasks is known to vary substantially across individuals (Parasuraman and Jiang, 2012). Each individual can adopt a different strategy to solve a task-problem, which is revealed in distinct brain activity patterns (Tavor et al., 2016). Individuals utilize different brain circuits, not only during working memory tasks but also during general cognitive tasks, and the degree to which this heterogeneity emerges is particularly pronounced for tasks involving higher-level cognitive functions (Barch et al., 2013; Jang et al., 2017). The results of PEB for all participants (Figure 5b) show that posterior estimates of B during N-back tasks have larger confidence intervals than estimates of A. This result implies that participants may share a common scaffold or backbone of intrinsic effective connectivity but exhibit very different task related changes in connectivity from subject to subject.

This inter-subject heterogeneity was more prominent in the task-driven effective connectivity than the resting-state intrinsic connectivity. In contrast to low modularity Q of A matrices during the resting-state (0.1871), the modularity Q of similarity matrix of B matrices of N-back tasks was 0.3922;

in the range from 0.3 to 0.7, which is typically known to form a strong community structure (Newman and Girvan, 2004). Participants exhibit three network phenotypes when performing the N-back task, speaking to the *network degeneracy* hypothesis introduced above. For example, the changes in connectivity in subgroup 2 are primarily from the right SPL, while subgroup 3 shows a selective enabling of effective connectivity primarily from the left SPL (see PEB estimates of B parameters from subgroups 2 and 3 in Figure 5c). An individual may adopt different strategies and engage different neural networks when performing tasks. In a previous study by Dima et al. (2014), there were several DCM architectures that could explain fMRI data for the 2-back tasks. This study implies involvement of distinct functional networks across individuals – for the working memory tasks studied here. A subtyping of working memory circuits was also found in the study of Brodersen et al. (2014), who showed three subgroups of schizophrenia following DCM of the N-back task, having significantly different symptom scores on standard (schizophrenia research) instruments.

In contrast, the modularity of similarity matrix of intrinsic connectivity during the resting-state did not show a strong community structure. This finding may be attributable to the conservation of intrinsic effective connectivity across individuals as a characteristic of intrinsic human brain networks.

Relation between connectivity changes and behavior

The relationship between the task-state and the resting-state networks has been studied by many to explain or predict behavioral performance. Sala-Llonch et al. (2012) showed that participants who exhibit a stronger negative correlation between the resting-state default mode network and working memory networks perform better in behavioral tasks. Elton and Gao (2014) also showed that dissociation between a network in resting-state and the connectivity from a selective attention task was positively correlated with task accuracy. In the current study, we found that similarities between the intrinsic connectivity of the N-back task and the task-related changes in effective connectivity were positively correlated with 3-back RTs. This result implies that faster responses (thus higher performance) are associated with a greater divergence of task-related connectivity from intrinsic connectivity during the N-back task. More specifically, the positive correlation between 3-back RTs and similarity between the task-related connectivity and the intrinsic resting-state connectivity was found for those participants with task-related effective connectivity from the parietal to the frontal regions (subgroups 2 and 3). As the effective connectivity during the N-back tasks deviates further from the intrinsic connectivity during the resting-state, participants, who had significant parieto-frontal connectivity, responded to stimuli faster. This relationship is found only in the difficult condition (3-back task) since the 2-back RTs did not show any significant relationship with this similarity measure. Therefore, it appears that performing difficult tasks requires a greater departure from the intrinsic network architecture for more efficient performance, particularly in individuals engaging parieto-frontal connectivity for N-back tasks.

DCM in 7 Tesla MRI

The data sets of resting-state and task-state fMRI were acquired at a relatively high magnetic field strength, 7 Tesla MRI. The activated regions during the N-back tasks were similar to the regions identified in previous studies that used the same experimental paradigm with the magnetic field of 1.5 Tesla (Dima et al., 2014) or 3 Tesla (Deserno et al., 2012). The modulatory or task-specific effect of N-back tasks on the connectivity from the parietal lobe to the frontal lobe observed in the current study was equivalently observed by the previous studies of N-back tasks performed at 1.5 Tesla (Dima et al., 2014). This suggests that DCM can consistently identify neural architectures underlying cognitive tasks regardless of different magnetic field strengths. We expect the differential effects of 3 Tesla and 7 Tesla on DCM will be explored further in future studies.

In this study, the driving input parameter C had a negative value. This means that the driving input reduces overall activity in the target regions; presumably through interactions between excitatory (e.g., spiny stellate) and inhibitory interneurons, in receipt of afferent driving input. Interestingly, the negative effective connectivity from the parietal regions to the frontal regions means that the frontal regions are effectively disinhibited by driving input. In other words, the input inhibits the inhibitory influences mediated by extrinsic (between-region) connections between the parietal and prefrontal regions. Finally, we modeled task-related effective connectivity changes in both 2-back and 3-back condition; to ensure more reliable parameter estimation. Thus, the effective connectivity described in this paper reflects a common circuit involved in both 2-back and 3-back processing.

In summary, we have (i) explored context-sensitive divergence of task-related effective connectivity from the intrinsic resting-state effective connectivity, (ii) examined phenotypes of effective connectivity across participants during tasks and (iii) have found strong association between behavioral performance and the degree with which intrinsic effective connectivity is reconfigured, in high-performing phenotypes. This suggests that the degree to which a task-dependent coupling in the brain diverges from task-free intrinsic coupling is associated with task performance.

Acknowledgement

This work was supported by a grant from the Korea Health Technology R&D Project through the Korea Health Industry Development Institute (KHIDI) funded by the Ministry of Health & Welfare, Republic of Korea (HI14C2444) (HJP) and the Wellcome Trust (KF). The authors thank Maengkeun Oh for his help with data pre-processing and Hanseul Choi for her help with the research on working memory.

References

Annett, M., 1970. A classification of hand preference by association analysis. Br J Psychol 61, 303-321.

Barch, D.M., Burgess, G.C., Harms, M.P., Petersen, S.E., Schlaggar, B.L., Corbetta, M., Glasser, M.F., Curtiss, S., Dixit, S., Feldt, C., Nolan, D., Bryant, E., Hartley, T., Footer, O., Bjork, J.M., Poldrack, R., Smith, S., Johansen-Berg, H., Snyder, A.Z., Van Essen, D.C., Consortium, W.-M.H., 2013. Function in the human connectome: Task-fMRI and individual differences in behavior. Neuroimage 80, 169-189.

Bernal-Casas, D., Balaguer-Ballester, E., Gerchen, M.P., Iglesias, S., Walter, H., Heinz, A., Meyer-Lindenberg, A., Stephan, K.E., Kirsch, P., 2013. Multi-site reproducibility of prefrontal-hippocampal connectivity estimates by stochastic DCM. Neuroimage 82, 555-563.

Biswal, B., Yetkin, F.Z., Haughton, V.M., Hyde, J.S., 1995. Functional connectivity in the motor cortex of resting human brain using echo-planar MRI. Magn Reson Med 34, 537-541.

Brodersen, K.H., Deserno, L., Schlagenhauf, F., Lin, Z.H., Penny, W.D., Buhmann, J.M., Stephan, K.E., 2014. Dissecting psychiatric spectrum disorders by generative embedding. Neuroimage-Clinical 4, 98-111.

Buxton, R.B., Wong, E.C., Frank, L.R., 1998. Dynamics of blood flow and oxygenation changes during brain activation: the balloon model. Magn Reson Med 39, 855-864.

Chang, C.-C., Lin, C.-J., 2011. LIBSVM: a library for support vector machines. ACM Transactions on Intelligent Systems and Technology (TIST) 2, 27.

Cole, M.W., Bassett, D.S., Power, J.D., Braver, T.S., Petersen, S.E., 2014. Intrinsic and task-evoked network architectures of the human brain. Neuron 83, 238-251.

Cole, M.W., Ito, T., Bassett, D.S., Schultz, D.H., 2016. Activity flow over resting-state networks shapes cognitive task activations. Nature Neuroscience 19, 1718-1726.

Corbetta, M., Patel, G., Shulman, G.L., 2008. The reorienting system of the human brain: from environment to theory of mind. Neuron 58, 306-324.

Daunizeau, J., Stephan, K.E., Friston, K.J., 2012. Stochastic dynamic causal modelling of fMRI data: should we care about neural noise? , Neuroimage, pp. 464-481.

Deserno, L., Sterzer, P., Wustenberg, T., Heinz, A., Schlagenhauf, F., 2012. Reduced Prefrontal-Parietal Effective Connectivity and Working Memory Deficits in Schizophrenia. Journal of Neuroscience 32, 12-20.

Dima, D., Jogia, J., Frangou, S., 2014. Dynamic causal modeling of load-dependent modulation of effective connectivity within the verbal working memory network. Human Brain Mapping 35, 3025-3035.

Edelman, G.M., Gally, J.A., 2001. Degeneracy and complexity in biological systems. Proc Natl Acad Sci U S A 98, 13763-13768.

Elton, A., Gao, W., 2014. Divergent task-dependent functional connectivity of executive control and salience networks. Cortex 51, 56-66.

Fonville, L., Kadosh, K.C., Drakesmith, M., Dutt, A., Zammit, S., Mollon, J., Reichenberg, A., Lewis, G., Jones, D.K., David, A.S., 2015. Psychotic Experiences, Working Memory, and the Developing Brain: A Multimodal Neuroimaging Study. Cerebral Cortex 25, 4828-4838.

Fox, M.D., Raichle, M.E., 2007. Spontaneous fluctuations in brain activity observed with functional magnetic resonance imaging. Nature Reviews Neuroscience 8, 700-711.

Friston, K., Zeidman, P., Litvak, V., 2015. Empirical Bayes for DCM: A Group Inversion Scheme. Front Syst Neurosci 9, 164.

Friston, K.J., Harrison, L., Penny, W., 2003. Dynamic causal modelling. Neuroimage 19, 1273-1302.

Friston, K.J., Kahan, J., Biswal, B., Razi, A., 2014. A DCM for resting state fMRI. Neuroimage 94, 396-407.

Friston, K.J., Li, B., Daunizeau, J., Stephan, K.E., 2011. Network discovery with DCM. Neuroimage 56, 1202-1221.

Friston, K.J., Litvak, V., Oswal, A., Razi, A., Stephan, K.E., van Wijk, B.C., Ziegler, G., Zeidman, P., 2016. Bayesian model reduction and empirical Bayes for group (DCM) studies. Neuroimage 128, 413-431.

Friston, K.J., Penny, W.D., Glaser, D.E., 2005. Conjunction revisited. Neuroimage 25, 661-667.

Friston, K.J., Price, C.J., 2003. Degeneracy and redundancy in cognitive anatomy. Trends Cogn Sci 7, 151-152.
Greicius, M.D., Krasnow, B., Reiss, A.L., Menon, V., 2003. Functional connectivity in the resting brain: A network analysis of the default mode hypothesis. Proceedings of the National Academy of Sciences of the United States of America 100, 253-258.
Harvey, P.O., Fossati, P., Pochon, J.B., Levy, R., Lebastard, G., Lehericy, S., Allilaire, J.F., Dubois, B., 2005. Cognitive control and brain resources in major depression: an fMRI study using the n-back task. Neuroimage 26, 860-869.
Hermundstad, A.M., Bassett, D.S., Brown, K.S., Aminoff, E.M., Clewett, D., Freeman, S., Frithsen, A., Johnson, A., Tipper, C.M., Miller, M.B., Grafton, S.T., Carlson, J.M., 2013a. Structural foundations of resting-state and task-based functional connectivity in the human brain. Proceedings of the National Academy of Sciences of the United States of America 110, 6169-6174.
Hermundstad, A.M., Bassett, D.S., Brown, K.S., Aminoff, E.M., Clewett, D., Freeman, S., Frithsen, A., Johnson, A., Tipper, C.M., Miller, M.B., Grafton, S.T., Carlson, J.M., 2013b. Structural foundations of resting-state and task-based functional connectivity in the human brain. Proc Natl Acad Sci U S A 110, 6169-6174.
Honey, G.D., Fu, C.H.Y., Kim, J., Brammer, M.J., Croudace, T.J., Suckling, J., Pich, E.M., Williams, S.C.R., Bullmore, E.T., 2002. Effects of verbal working memory load on corticocortical connectivity modeled by path analysis of functional magnetic resonance imaging data. Neuroimage 17, 573-582.
Jang, C., Knight, E.Q., Pae, C., Park, B., Yoon, S.A., Park, H.J., 2017. Individuality manifests in the dynamic reconfiguration of large-scale brain networks during movie viewing. Scientific Reports 7.
Krienen, F.M., Yeo, B.T.T., Buckner, R.L., 2014. Reconfigurable task-dependent functional coupling modes cluster around a core functional architecture. Philosophical Transactions of the Royal Society B-Biological Sciences 369.
Leicht, E.A., Newman, M.E.J., 2008. Community structure in directed networks. Physical Review Letters 100.
Li, B., Daunizeau, J., Stephan, K.E., Penny, W., Hu, D., Friston, K., 2011. Generalised filtering and stochastic DCM for fMRI. Neuroimage 58, 442-457.
Lowe, M.J., Mock, B.J., Sorenson, J.A., 1998. Functional connectivity in single and multislice echoplanar imaging using resting-state fluctuations. NeuroImage 7, 119-132.
Manelis, A., Reder, L.M., 2014. Effective connectivity among the working memory regions during preparation for and during performance of the n-back task. Frontiers in Human Neuroscience 8.
McGuire, P.K., Paulesu, E., Frackowiak, R.S., Frith, C.D., 1996. Brain activity during stimulus independent thought. Neuroreport 7, 2095-2099.
Newman, M.E.J., Girvan, M., 2004. Finding and evaluating community structure in networks. Physical Review E 69.
Owen, A.M., McMillan, K.M., Laird, A.R., Bullmore, E.T., 2005. N-back working memory paradigm: A meta-analysis of normative functional neuroimaging. Human Brain Mapping 25, 46-59.
Papma, J.M., den Heijer, T., de Koning, I., Mattace-Raso, F.U., van der Lugt, A., van der Lijn, F., van Swieten, J.C., Koudstaal, P.J., Smits, M., Prins, N.D., 2012. The influence of cerebral small vessel disease on default mode network deactivation in mild cognitive impairment. Neuroimage Clin 2, 33-42.
Parasuraman, R., Jiang, Y., 2012. Individual differences in cognition, affect, and performance: Behavioral, neuroimaging, and molecular genetic approaches. Neuroimage 59, 70-82.
Park, B., Kim, D.-S., Park, H.-J., 2014. Graph Independent Component Analysis Reveals Repertoires of Intrinsic Network Components in the Human Brain. PLoS ONE 9, e82873.
Park, H.J., Chun, J.W., Park, B., Park, H., Kim, J.I., Lee, J.D., Kim, J.J., 2011. Activation of the occipital cortex and deactivation of the default mode network during working memory in the early blind. J Int Neuropsychol Soc 17, 407-422.
Park, H.J., Friston, K., 2013. Structural and functional brain networks: from connections to cognition. Science 342, 1238411.
Price, C.J., Friston, K.J., 1997. Cognitive conjunction: a new approach to brain activation experiments. Neuroimage 5, 261-270.
Price, C.J., Friston, K.J., 2002. Degeneracy and cognitive anatomy. Trends Cogn Sci 6, 416-421.

Raichle, M.E., Snyder, A.Z., 2007. A default mode of brain function: a brief history of an evolving idea. NeuroImage 37, 1083-1090; discussion 1097-1089.
Rubinov, M., Sporns, O., 2010. Complex network measures of brain connectivity: uses and interpretations. Neuroimage 52, 1059-1069.
Sala-Llonch, R., Pena-Gomez, C., Arenaza-Urquijo, E.M., Vidal-Pineiro, D., Bargallo, N., Junque, C., Bartres-Faz, D., 2012. Brain connectivity during resting state and subsequent working memory task predicts behavioural performance. Cortex 48, 1187-1196.
Schmidt, A., Smieskova, R., Simon, A., Allen, P., Fusar-Poli, P., McGuire, P.K., Bendfeldt, K., Aston, J., Lang, U.E., Walter, M., Radue, E.W., Riecher-Rossler, A., Borgwardt, S.J., 2014. Abnormal effective connectivity and psychopathological symptoms in the psychosis high-risk state. Journal of Psychiatry & Neuroscience 39, 239-248.
Smith, S.M., Fox, P.T., Miller, K.L., Glahn, D.C., Fox, P.M., Mackay, C.E., Filippini, N., Watkins, K.E., Toro, R., Laird, A.R., Beckmann, C.F., 2009. Correspondence of the brain's functional architecture during activation and rest. Proceedings of the National Academy of Sciences of the United States of America 106, 13040-13045.
Stephan, K.E., Weiskopf, N., Drysdale, P.M., Robinson, P.A., Friston, K.J., 2007. Comparing hemodynamic models with DCM. Neuroimage 38, 387-401.
Tavor, I., Jones, O.P., Mars, R.B., Smith, S.M., Behrens, T.E., Jbabdi, S., 2016. Task-free MRI predicts individual differences in brain activity during task performance. Science 352, 216-220.
Tononi, G., Sporns, O., Edelman, G.M., 1999. Measures of degeneracy and redundancy in biological networks. Proc Natl Acad Sci U S A 96, 3257-3262.
Yeo, B.T.T., Krienen, F.M., Eickhoff, S.B., Yaakub, S.N., Fox, P.T., Buckner, R.L., Asplund, C.L., Chee, M.W.L., 2015. Functional Specialization and Flexibility in Human Association Cortex. Cerebral Cortex 25, 3654-3672.